Article

Bacterial Footprints in Elastic Pillared Microstructures

Susarrey-Arce, Arturo, Hernández-Sánchez, José Federico, Marcello, Marco, Diaz-Fernandez, Yuri, Oknianska, Alina, Sorzabal-Bellido, Ioritz, Tiggelaar, Roald, Lohse, Detlef, Gardeniers, Han, Snoeijer, Jacco, Marin, Alvaro and Raval, Rasmita

Susarrey-Arce, Arturo, Hernández-Sánchez, José Federico, Marcello, Marco, Diaz-Fernandez, Yuri, Oknianska, Alina, Sorzabal-Bellido, Ioritz, Tiggelaar, Roald, Lohse, Detlef, Gardeniers, Han et al (2018) Bacterial Footprints in Elastic Pillared Microstructures. ACS Applied Bio Materials, 1 (5). pp. 1294-1300. ISSN 2576-6422

http://dx.doi.org/10.1021/acsabm.8b00176

ACS APPLIED BIO MATERIALS

Article

www.acsabm.org

Bacterial Footprints in Elastic Pillared Microstructures

Arturo Susarrey-Arce,[*,†,○] José Federico Hernández-Sánchez,[*,‡,○] Marco Marcello,[¶] Yuri Diaz-Fernandez,[†] Alina Oknianska,[§] Ioritz Sorzabal-Bellido,[†] Roald Tiggelaar,[∥] Detlef Lohse,[⊥] Han Gardeniers,[#] Jacco Snoeijer,[*,⊥] Alvaro Marin,[⊥] and Rasmita Raval[*,†]

[†]Open Innovation Hub for Antimicrobial Surfaces at the Surface Science Research Centre and Department of Chemistry, University of Liverpool, Oxford Street, Liverpool L69 3BX, United Kingdom

[‡]Division of Physical Sciences and Engineering and Clean Combustion Research Center, King Abdullah University of Science and Technology, Thuwal 23955-6900, Saudi Arabia

[¶]Institute of Integrative Biology, University of Liverpool, Biosciences Building, Liverpool L69 7ZB, United Kingdom

[§]School of Health Sciences, Liverpool Hope University, Hope Park, Liverpool L16 9JD, United Kingdom

[∥]NanoLab Cleanroom, MESA+ Institute for Nanotechnology, University of Twente, P.O. Box 217, Enschede 7500AE, The Netherlands

[⊥]Physics of Fluids Group, MESA+ Institute for Nanotechnology, J.M. Burgers Centre for Fluid Dynamics, University of Twente, P.O. Box 217, Enschede 7500AE, The Netherlands

[#]Mesoscale Chemical Systems, MESA+ Institute for Nanotechnology, University of Twente, P.O. Box 217, Enschede 7500AE, The Netherlands

Supporting Information

ABSTRACT: Soft substrates decorated with micropillar arrays are known to be sensitive to deflection due to capillary action. In this work, we demonstrate that micropillared epoxy surfaces are sensitive to single drops of bacterial suspensions. The micropillars can show significant deformations upon evaporation, just as capillary action does in soft substrates. The phenomenon has been studied with five bacterial strains: *S. epidermidis*, *L. sakei*, *P. aeruginosa*, *E. coli*, and *B. subtilis*. The results reveal that only droplets containing motile microbes with flagella stimulate micropillar bending, which leads to significant distortions and pillar aggregations forming dimers, trimers, and higher order clusters. Such deformation is manifested in characteristic patterns that are left on the microarrayed surface following evaporation and can be easily identified even by the naked eye. Our findings could lay the ground for the design and fabrication of mechanically responsive substrates, sensitive to specific types of microorganisms.

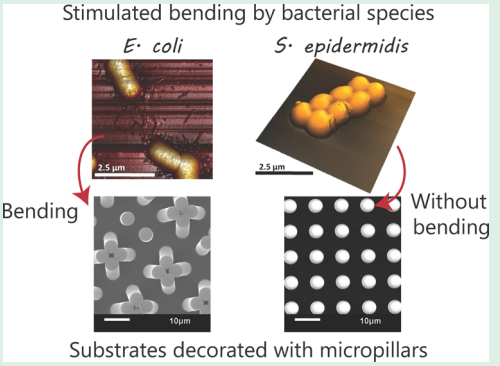

KEYWORDS: *bacteria, bending, elastic micropillars, capillarity, responsive substrates*

INTRODUCTION

The fabrication of materials that are sensitive to physical, chemical, or biological stimuli has opened opportunities for the development of a wide variety of technological applications such as switchable adhesion, mechanosensing, and stimuli-responsive materials.[1−6] In particular, the design of biomimetic structures,[3,7] inspired by natural systems, has been a powerful tool in the implementation of smart, artificial systems.[8,9] In this respect, the use of topographic surfaces is particularly interesting, with natural systems utilizing physical structures, from the nano- to the macroscale, to deliver functions such as superhydrophobicity, adhesion, and antibiofouling as demonstrated by the lotus leaf, shark skin, and gecko feet.[4,7,9−13]

There has been particular interest in developing mechanically responsive systems.[8,14] An excellent example is the mechanical response of micropillar arrays upon drying of water (or water-based solutions).[15−26] When water droplets evaporate on relatively soft elastic microstructured surfaces, capillary action can generate a significant force that is able to bend the soft micropillars. Depending on the geometry of the arrays, the capillary and elastic forces can form different pillar assemblies.[15,16] The complexity of the assemblies varies with the pillar height and the interpillar distance. For example, large periodic chiral aggregates can be formed when the micropillars are higher and closer to each other. Each cluster of aggregates has a different potential to store elastic energy, embody information, enhance adhesion, or capture particles.[17,18]

Received: May 31, 2018
Accepted: October 15, 2018
Published: October 15, 2018

DOI: 10.1021/acsabm.8b00176
ACS Appl. Bio Mater. XXXX, XXX, XXX−XXX

The demonstration of mechanically responsive topographic surfaces to bacterial stimuli during evaporation of small droplets is of great interest and has not been demonstrated before. Furthermore, the deflections seen in our systems are significant, leading to pillar aggregations into dimers, trimers, and higher order clusters. Recently, the formation of biofilm strings and networks between topographic pillars has been demonstrated in liquid media;[27] however, the mechanical response of the pillars to bacterial presence upon evaporation is not observed. Chew and coauthors have shown small deflections of macropillared surfaces in response to the differential pressure exerted by biofilm growth within a growth chamber over a 24 h period,[28] while Biais[29] and Ng[30] et al. have investigated the interaction of bacterial pili with pillared structures.

Here, we demonstrate how epoxy-made soft surfaces containing micropillar arrays interact with suspensions of different bacterial species. Our results suggest that the presence of motile bacteria with flagella drastically increases the mechanical response of the pillars, actively bending soft topographical substrates in the area contained within the contact line. In contrast, solutions containing nonmotile bacteria do not generate such responses. We attribute this to the ability of motile bacteria to interact with each other and with their topographical environment. Importantly, the response of the microarray is sensitive to the type and concentration of bacteria in the solution. These promising results could lay the foundation for the development of devices that are selectively responsive to specific microorganisms, paving the way to construct smart, fast, and cost-effective diagnostic tools.

RESULTS AND DISCUSSION

One of the key parameters in the mechanical response of soft micropillar arrays is the aspect ratio of a single pillar. We investigated the effect of the pillar aspect ratio by fabricating regular patterns of cylindrical pillars with a constant diameter (5 μm) and interspacing (5 μm) and with variable height (from 5 to 45 μm). The patterns were created on epoxy resin using a method described before[31−35] based on casting uncured epoxy on a negative polydimethilsiloxane (PDMS) mold, followed by curing and mechanically removing of the mold. The micropatterns were transferred efficiently, with a high degree of fidelity, as shown by scanning electron microscopy (SEM) imaging (Figure 1 and Figure S1).

These microstructured substrates can be susceptible to elastocapillary forces in the presence of pure liquids. Therefore, we evaluated the effect of pure water over a surface decorated with micropillars with lengths varying from 5 to 45 μm (Figure 1) during the evaporation of water droplets (Figure 1). In these experiments, the liquid filled up the space between the pillars, resulting in an almost square-shaped droplet contour. Once the droplet spreads on the substrate, the liquid contact line is blocked by the pillared structure and remains immobilized (pinned) for the rest of the drying process.[31] Figure 1b shows that after complete evaporation, there is almost no trace of the droplet, except at the droplet contour, where lines of pillars were bent by capillary action at the contact line shown in Video S1.[18−23,31]

In the systems studied, the pillar lattice was kept constant (i.e., $l = d = 5$ μm), but different pillar heights (h) ranging from $h = 5$ to 45 μm were fabricated. Thus, a range of micropatterned surfaces were generated with different aspect ratios (i.e., $h/d = 3$ to $h/d = 9$). For large aspect ratio structures, we observed significant perturbation of the micropillars in the area within the contact line boundary. Imaging at low magnifications, or even examination by the naked eye, revealed that the inner part of the pattern was opaque, suggesting that the whole array of pillars inside the dried droplet perimeter was modified (Figure 1c). Higher magnification SEM imaging showed that this optical contrast

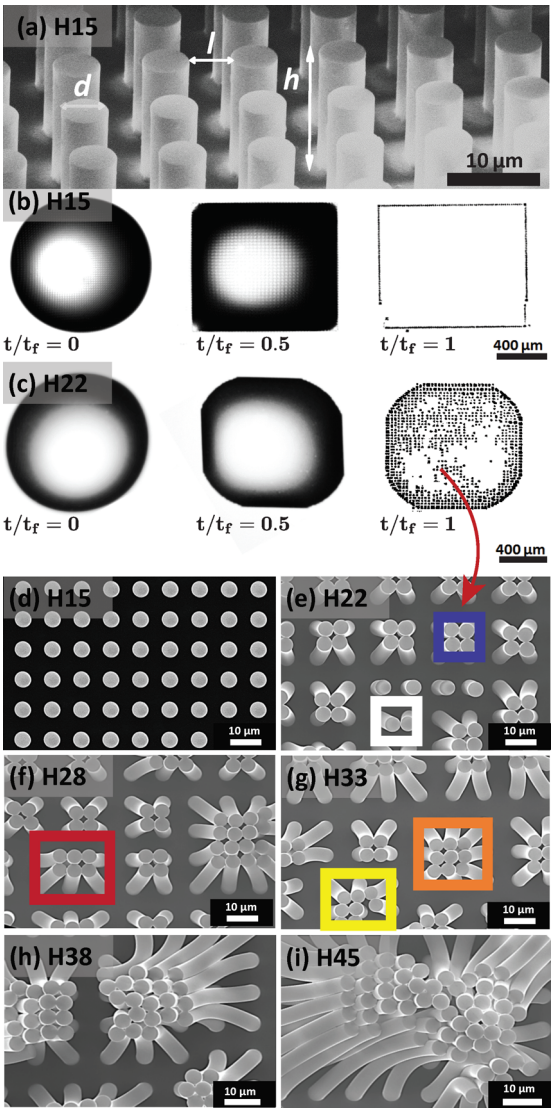

Figure 1. (a) Representative SEM image of pillared structure (H15), showing the topographic descriptors for the array. The pillars have a cylindrical shape and a height (h) of 15 μm and a diameter (d) of 5 μm forming a square lattice with an interpillar distance (l) = 5 μm. (b) Pure water droplet evaporating on the H15 substrate with micropillars leaving a distinct square-shaped contact line with no perturbation of pillars within this contour. (c) Pure water droplet evaporating on the H22 substrate with micropillars leaving a distinct shaped contact line pattern with significant modification of the micropillars within the contact line boundary. Time needed is represented in a dimensionless form as the ratio between the elapsed time (t) and the final evaporation time (t_f). (d–i) Pillared structures with constant ($d = 5$ μm) and different pillar heights (h) of (d) 15 μm (H15), (e) 22 μm (H22), (f) 28 μm (H28), (g) 33 μm (H33), (h) 38 μm (H38), and (i) 45 μm (H45). SEM images are presented for the different heights after evaporation of pure water droplets, probing the sensitivity of the structures to pure elastocapillary bending.

DOI: 10.1021/acsabm.8b00176
ACS Appl. Bio Mater. XXXX, XXX, XXX−XXX

effect was caused by local bending of the micropillars (Figure 1d–i), with the pillars bent toward each other forming clusters and adopting complex geometries, e.g., dimer (white box), tetramer (blue box), hexamer (red box), octamer (yellow box), and nonamer (orange box). Similar effects have been reported before for larger pillar aspect ratios[18,24,25] and were attributed to the elastocapillary coalescence of the flexible structures.[15,18] In our experiments, as the aspect ratio decreased, the clusters contained lower numbers of aggregated pillars until a critical aspect ratio $h/d = 3$, for which no clusters were observed in the inner part of the droplet (Figure 1d).

The deformation of the pillars, upon water evaporation, is induced by the surface tension (γ) of the water/air meniscus connecting the pillars, and the corresponding force scales as $F_c \sim \gamma r$, where $r = d/2$ is the pillar radius.[21,36] The natural elasticity of the pillars resists deformation with an elastic force $F_E \sim Elr^4/h^3$, where E is the Young modulus and l the interpillar distance.[18] This expression is analogous to the usual beam theory for slender objects, showing that the resistance to bending decreases strongly when the pillars height increases. If we define the pillar bending sensitivity as the ratio of capillary and elastic forces, $F_c/F_E = \gamma/El(h/r)^3$, we can conclude that it is directly proportional to the cubic power of the pillar aspect ratio h/r; i.e., slender pillars are more prone to be bent by surface tension, while wide pillars tend to be more stable.

Under our experimental conditions, no pillar coalescence is observed in the area within the contact line boundary from pure water when the aspect ratio is below $h/d = 3$,[31] suggesting that this is the critical aspect ratio threshold for which capillary action equals restoration mechanical stress on the micropillars. It is important to note that in this analysis, we are not considering the effect of the contact line. This effect is expected to have an enhanced deforming effect, but an accurate evaluation of this factor is beyond existing phenomenological modeling capabilities and will be the subject of future studies. Consequently, all of the results described below applies exclusively to the inner part of the dried pattern left by the droplet, ignoring possible contact line effects.

Bacterial-Triggered Coalescence of Pillars. From the elastocapillary assay discussed in the previous section, we identified the critical region within the topographic parameter space where the micropillared structure is able to resist capillary deformation in the presence of pure water droplets. Such a surface opens up the possibility to sense the presence of a second entity introduced into water (i.e., bacterial cells), which could induce a response in its own right. This critical structure corresponds to an aspect ratio $h/d \approx 3$ and pillar height $h = 15$ μm (H15, Figure 1d), as discussed in the previous section.

We, therefore, investigated the drying process of droplets containing different bacteria species over the H15 pillared structures. Similar to the case of pure water droplets, a pinned square drop shape is found. However, the patterns observed within the contact line formed after complete evaporation of the droplets were surprisingly different for some bacteria as clearly observed in Video S2.

Five different bacterial species, with a wide range of morphological and biological characteristics were investigated: *S. epidermidis*, *L. sakei*, *P. aeruginosa*, *E. coli*, and *B. subtilis*. The patterns formed after evaporation of droplets containing different bacteria on H15 pillar substrates (Figure 2) can be classified in two main groups: one group displaying significant bending of the pillars within the pattern (*P. aeruginosa*, *E. coli*, and *B. subtilis*) and another group that does not induce any responsive bending of the pillars in the center of the dried patterns (*S. epidermidis* and *L. sakei*). These distinct behaviors could be observed even by the naked eye in the form of a local change in contrast at the surface (Figure 2, 5×). At higher magnifications, the difference is clearly revealed to be associated with the coalescence of adjacent pillars (Figure 2, 40× and SEM (100×)).

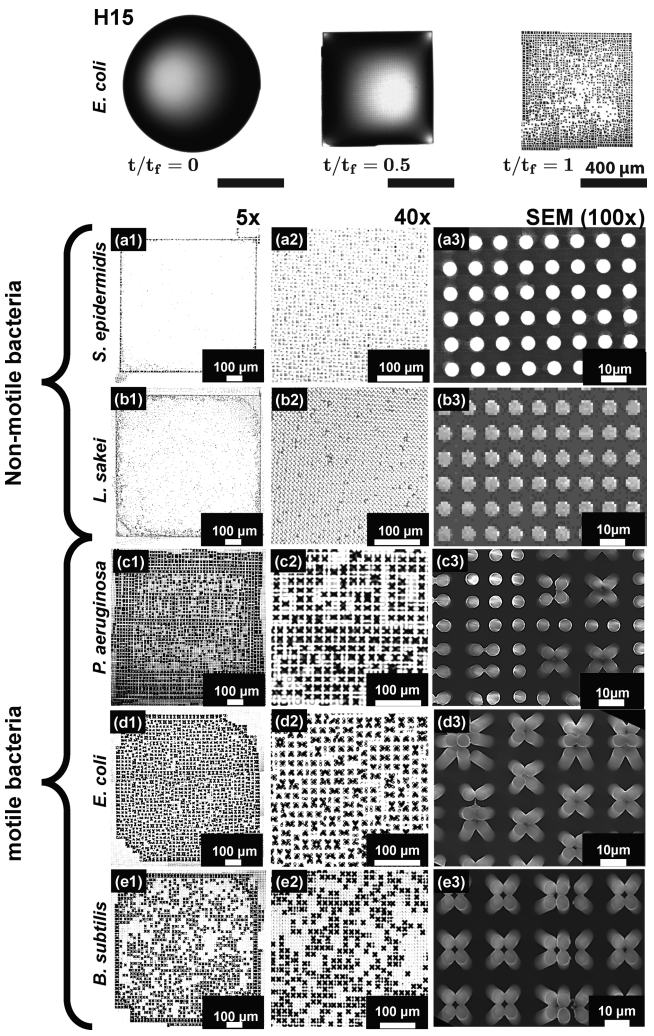

Figure 2. Typical patterns left over H15 substrates after the evaporation of different bacterial species: (a1–a3) *S. epidermidis*, (b1–b3) *L. sakei*, (c1–c3) *P. aeruginosa*, (d1–d3), *E. coli*, (e1–e3) *B. subtilis*. Here, the concentration of the different bacterial species is 10^7 CFU/mL. The different columns correspond to different degrees of magnifications: 5× (left column), 40× (central column) by using a confocal microscope, and >100× with SEM (right column).

We attempted to correlate these results to the general characteristics of the bacterial species used in this work (Table 1). Atomic force microscopy (AFM) imaging confirmed the expected size and cell morphology for these bacteria: Gram-negative (−) *P. aeruginosa* and *E. coli* as well as Gram-positive (+) *B. subtilis* and *L. sakei* present a rod-like shape, while Gram-positive (+) *S. epidermidis* has a spheroidal shape (Figure S2). In addition, *L. sakei* and *S. epidermidis* are not motile (no flagella present), while the other three strains have flagella. From these considerations, we can conclude that the different pattern types showed in Figure 2 (bending vs nonbending) cannot be explained considering bacteria cell

DOI: 10.1021/acsabm.8b00176
ACS Appl. Bio Mater. XXXX, XXX, XXX–XXX

Table 1. General Characteristics of the Different Bacterial Strains Used in the Study[a]

strain	gram	shape	$L \times W_a$ (μm^2)	flagella
(a) *P. aeruginosa*	−	rod	1.4(±0.2) × 0.8(±0.2)	yes
(b) *E. coli*	−	rod	1.7(±0.2) × 0.9(±0.2)	yes
(c) *B. subtilis*	+	rod	1.8(±0.4) × 0.80(±0.2)	yes
(d) *L. sakei*	+	rod	1.5(±0.4) × 0.8(±0.2)	no
(e) *S. epidermidis*	+	spherical	1.3(±0.3) × 1.3(±0.3)	no

[a]AFM images of cells are presented in Figure S2.

morphology only. Similarly, the stiffness of the cell envelop does not appear to play a critical role, with rigid Gram-positive bacteria and softer Gram-negative bacteria distributed among both pattern groups.

Interestingly, the different response of the microstructures upon evaporation of the bacterial solutions correlates with the presence or absence of flagella. Bacteria with flagella clearly induce a bending response in the H15 pillars, while nonflagellated bacteria are unable to bend the pillars when used at the same bacterial concentration.

For the bacteria that induce a mechanical response, a concentration dependence is observed, with deformation of pillar clusters at the center of the dried droplet observed for bacteria concentrations between 10^7 CFU/mL and 10^9 CFU/mL, while none is observed for lower bacteria concentrations (10^5 CFU/mL). At low concentrations, only the perimeter near the corners of the dried square pattern presented coalescence of the pillars (Figure 3a−c). This can be attributed to the coffee-stain-like effect, able to drag bacterial cells toward the droplet contact line, increasing the local concentration of bacteria during evaporation.[31] Interestingly, bacterial cells without flagella confirm the absence of responsivity at different cell concentrations (Figure 3d−f).

No clear correlation was observed between bacterial species and the cluster symmetries obtained (e.g., dimer, trimer, tetramer, etc.). However, the data suggests that the assemblies emerge due to perturbation of the balance between capillary forces and elastic restoration forces in the presence of bacteria with flagella. In the next section, we discuss a possible mechanism for this distinctive behavior.

Possible Origin of Bacteria-Induced Coalescence. In the previous sections, we determined the critical pillar aspect ratio, below which surface tension forces were not able to induce pillar coalescence in pure water. Interestingly, the responsivity is dramatically enhanced when the droplets contain flagellated bacteria. While the bending process at the perimeter of the contact line appears similar in both cases, coalescence within the central area is triggered at smaller aspect ratios by the presence of bacteria with flagella. This enhanced pillar bending effect results in characteristic patterns on the substrate, distinct for motile and nonmotile bacteria.

The possible origin of the enhanced pillar bending may be related to the ability of the bacteria with flagella to adhere to more than one pillar (Figure S3), thus connecting adjacent pillars and inducing a mechanical deformation. In the presence of bacteria with flagella, we observed, at SEM, after drying, structures bridging bent pillars, while nonflagellated bacteria appeared attached to single pillars. The morphology of the single bacterial cells cannot be distinguished, probably due to distortions on the cell envelop after evaporation, in the absence of fixation.

These effects can also be understood by comparing the length scales of bacterial structures and pillar interspacing distances. The average size of the capsule for a single bacterial cell is below 2 μm (Table 1), while flagella can reach tens of μm beyond the outer cell membrane.[37] Considering that in our microstructured surfaces the interpillar distance was 5 μm, bacteria without flagella will predominantly fall between the

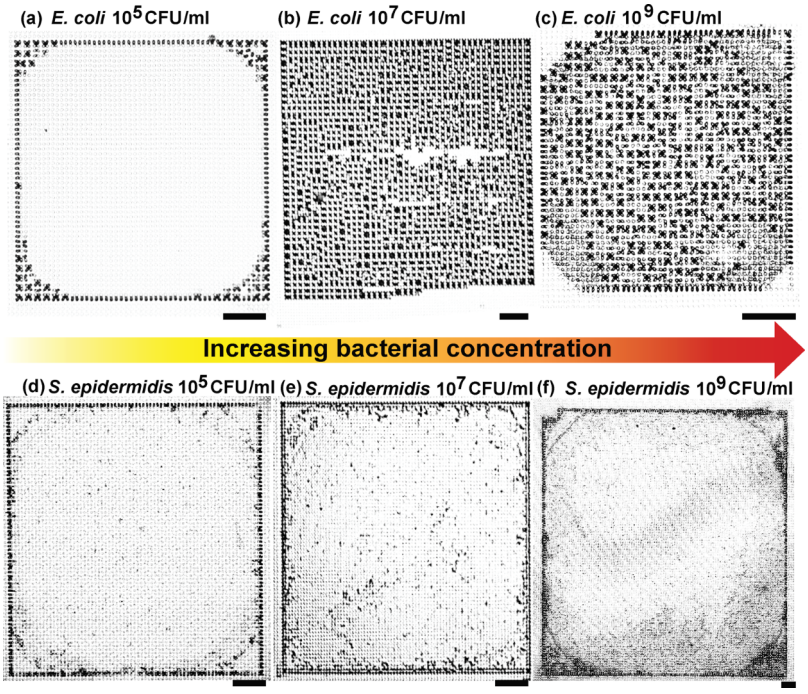

Figure 3. Effect of bacteria concentration on the bending pattern for *E. coli* and *S. epidermidis* on the H15 pillared substrate. Representative optical microscopy images for (a) 10^5 CFU/mL, (b) 10^7 CFU/mL, and (c) 10^9 CFU/mL. Scale bar in panels a−f is 100 μm.

DOI: 10.1021/acsabm.8b00176
ACS Appl. Bio Mater. XXXX, XXX, XXX−XXX

pillars or strongly adhere[38] to single pillars. On the other hand, bacteria with flagella,[32] in which appendage sizes exceed the interpillar distance, can potentially interact with more than one pillar, leading to the observed pillar deformation.

In support of this, we found evidence of bacterial matter residing between the bent pillars, after complete evaporation of droplets containing flagellated bacteria (Figure 4). Non-flagellated bacteria, on the other hand, are found attached to individual pillars only, forming nonconnecting structures (see Figures S4–S7).

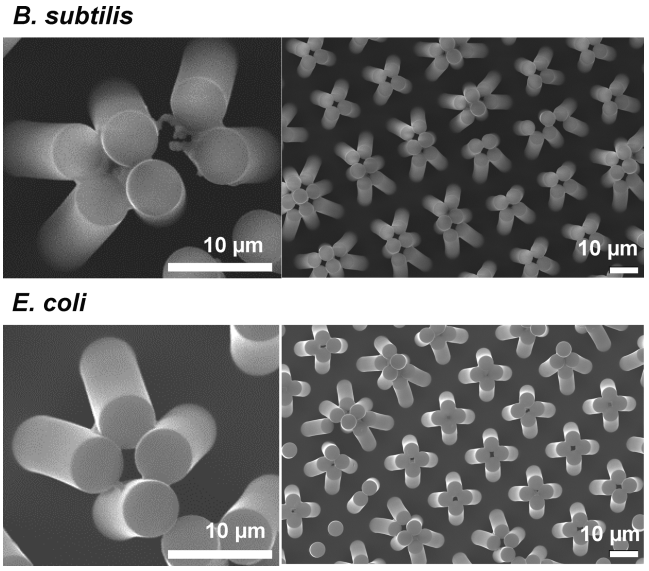

Figure 4. Representative SEM images of H15 pillared structures after drying of bacterial suspensions, showing motile bacteria (*B. subtilis* and *E. coli*) bridging the bent pillars. The concentration of the different bacterial species is 10^7 CFU/mL.

Although a more detailed investigation of bacterial behavior during the actual drying process is necessary to confirm the hypothesis proposed, our results support the potential use of pillared soft substrates to discriminate between motile and nonflagellated bacteria using a cost-effective and immediate assay based on droplet-drying, which can be performed and quickly analyzed by the naked eye. In addition, discrimination of bacterial concentration is also possible, with only samples containing concentrations above a critical threshold producing a response. We envision that by tuning the properties of the substrates, a more subtle differentiation between different microorganisms and different bacterial concentrations could be achieved in the future with this presented novel, easy to fabricate, and cost-effective technology.

CONCLUSIONS

We show that soft micropillared surfaces can be tailor-made sensitive to the presence of isolated bacterial cells in a single drop. The evaporation of water droplets and bacterial suspensions over fabricated micropillar arrays leads to very distinct micropillar deformations and patterns. Once the threshold for elastocapillary pillar coalescence is found, we observe that only bacteria with flagella can promote pillar coalescence. Such responsive micropillared surfaces could provide a platform for the development of fast and cost-effective self-responsive surfaces for bacterial detection and differentiation.

EXPERIMENTS AND METHODS

The epoxy micropillars were fabricated by casting EPO-TEK OG142-13 from Epoxy Technology into a negative replica PDMS mold, as described.[31,32] After the resin was casted, a 1.1 mm thick glass slide was placed over the mold and placed below an ultraviolet light for 20 min until the epoxy pillar was cured. The epoxy micropillars were mechanically removed from the mold. The SEM images of the epoxy pillars are shown in Figure S1. After the sample preparation, we measured the Young modulus (E) of the bulk material and the micropillar via an axial compression test. The E value for the bulk material was 1 ± 0.3 GPa, and the E value for the H15 substrate was 0.5 ± 0.2 GPa.

Bacterial cultures were performed following recommended growing conditions for each species. *P. aeruginosa* ATCC-8626, *E. coli* ATCC-10798, and *S. epidermidis* ATTC-12228 were grown overnight at 37 °C in liquid broth medium (Oxoid Ltd., Thermo Fisher). *B. subtilis* subsp. *subtilis* ATCC-6051 and *L. sakei* DSMZ-20017 were grown overnight at 30°C in MRS broth medium from Oxoid Ltd., Thermo Fisher. All of the cells cultures were then centrifuged and redispersed in sterile deionized water two times, finally adjusting the bacterial concentration to 10^7 colony-forming units per milliliter (CFU/mL), unless differently specified. Note that colony counting was performed after cell redispersion in deionized water to ensure cell viability.

The evaporation of all droplets was carried out placing a droplet of 5−10 μL ± 4 μL on the epoxy substrates. For droplets containing bacteria, experiments were performed in triplicates drying 5 droplets over substrates independently. The images were collected with a CMOS camera PCO Sensicam at 1 frames per second (fps). The droplet completely evaporated in approximately 2100 ± 300 s. Evaporation experiments were assessed at room temperature (21 ± 3 °C) in an atmosphere with a relative humidity of 35 ± 5%.

The contact angle measurements of water and bacterial suspension droplets on epoxy surfaces were carried out by placing a water droplet with bacterial suspension of 10^7 CFU/mL on the epoxy substrates. The contact angle (CA) for H15 was 100° ± 7°, whereas the CA was 92° ± 5° for H22, H28, and H33. For longer pillars like H38 and H45, the CA was 88° ± 3°. CA hysteresis was carried out in a similar manner as CA measurements but by tilting the substrate 45°. Experiments were performed for the H15 substrate with and without bacterial containing droplets only, the CA hysteresis was 50° ± 8°. No significant differences in CA and CA hysteresis were observed between water droplets and the deposited bacterial containing droplets. CA values are shown in Table S1.

Transmission light microscopy images of the dried patterns were collected with a Zeiss 510 confocal microscope equipped with ×10, ×20, and ×40 air objectives. AFM measurements from the Supporting Information were obtained using a Bruker Multimode 8 and a Keysights 5500 instrument. Prior to AFM morphological analysis, a droplet of bacteria suspension (10^7 CFU/mL) was deposited onto an oxygen plasma-treated epoxy flat substrate and dried at room temperature. Estimated length (L) × width (W_a) in Table 1 are reported within a standard deviation of 10−25% obtained by measuring 15−20 cells per bacterial strains. These tests were carried out independently in triplicates. Top-view scanning electron microscopy (SEM) imaging was performed at 20 kV. Side-view SEM was recorded after fracturing the epoxy/glass with a diamond cutter at accelerating voltages of 3 kV. Prior to SEM inspection in a JSM-6610 JEOL system, all samples were coated with 20 nm of chromium to increase the electrical conductivity. SEM images are presented without fixation, which involves several solvent exchange steps[39] preserving the bacterial footprints after droplet evaporation.

ASSOCIATED CONTENT

Supporting Information

The Supporting Information is available free of charge on the ACS Publications website at DOI: 10.1021/acsabm.8b00176.

SEM images of some of the pillared arrays fabricated; AFM images of bacterial cells dried over flat epoxy

DOI: 10.1021/acsabm.8b00176
ACS Appl. Bio Mater. XXXX, XXX, XXX−XXX

surfaces; close-ups of *E.coli* dried over the H15 pillared substrate; additional SEM images of bacteria on H15 pillared structures; contact angle values for water and bacterial suspensions on different pillared structures (PDF)

Video S1: droplet contour impalement (AVI)

Video S2: pillar bending by *B. subtilis* at the latest stages of evaporation (AVI)

AUTHOR INFORMATION

Corresponding Authors

*E-mail: A.Susarrey-Arce@liverpool.ac.uk.

*E-mail: Jose.HernandezSanchez@kaust.edu.sa.

*E-mail: j.h.snoeijer@utwente.nl.

*E-mail: r.raval@liverpool.ac.uk.

ORCID

Arturo Susarrey-Arce: 0000-0003-2572-223X

Detlef Lohse: 0000-0003-4138-2255

Han Gardeniers: 0000-0003-0581-2668

Author Contributions

○A.S.-A. and J.F.H.-S. contributed equally to this work

Notes

The authors declare no competing financial interest.

ACKNOWLEDGMENTS

We would like to thank Dr. Joanna Wnetrzak and the Liverpool Centre for Cell Imaging (CCI) for help with experimental design and technical support. We also acknowledge the support of the Nanoinvestigation Centre at University of Liverpool (NICAL) for access to the SEM facility. Stefan Schlautmann (Mesoscale Chemical Systems, MESA+ Institute of Nanotechnology, University of Twente) is also acknowledged for sample fabrication. This work was partly funded by BBSRC (BB/R012415/1).

REFERENCES

(1) Tawfick, S.; De Volder, M.; Copic, D.; Park, S. J.; Oliver, C. R.; Polsen, E. S.; Roberts, M. J.; Hart, A. J. Engineering of Micro-and Nanostructured Surfaces with Anisotropic Geometries and Properties. *Adv. Mater.* **2012**, *24*, 1628−1674.

(2) Le, V.; Lee, J.; Chaterji, S.; Spencer, A.; Liu, Y.-L.; Kim, P.; Yeh, H.-C.; Kim, D.-H.; Baker, A. B. Syndecan-1 in Mechanosensing of Nanotopological Cues in Engineered Materials. *Biomaterials* **2018**, *155*, 13−24.

(3) Chakrapani, N.; Wei, B.; Carrillo, A.; Ajayan, P. M.; Kane, R. S. Capillarity-Driven Assembly of Two-Dimensional Cellular Carbon Nanotube Foams. *Proc. Natl. Acad. Sci. U. S. A.* **2004**, *101*, 4009−4012.

(4) Boesel, L. F.; Greiner, C.; Arzt, E.; Del Campo, A. Gecko-Inspired Surfaces: a Path to Strong and Reversible Dry Adhesives. *Adv. Mater.* **2010**, *22*, 2125−2137.

(5) Prieto-López, L.; Williams, J. Using Microfluidics to Control Soft Adhesion. *J. Adhes. Sci. Technol.* **2016**, *30*, 1555−1573.

(6) Prieto-López, L. O.; Williams, J. A. Switchable Adhesion Surfaces with Enhanced Performance Against Rough Counterfaces. *Biomimetics* **2016**, *1*, 2.

(7) Kwak, M. K.; Jeong, H.-E.; Kim, T.-i.; Yoon, H.; Suh, K. Y. Bio-Inspired Slanted Polymer Nanohairs for Anisotropic Wetting and Directional Dry Adhesion. *Soft Matter* **2010**, *6*, 1849−1857.

(8) Trichet, L.; Le Digabel, J.; Hawkins, R. J.; Vedula, S. R. K.; Gupta, M.; Ribrault, C.; Hersen, P.; Voituriez, R.; Ladoux, B. Evidence of a Large-Scale Mechanosensing Mechanism for Cellular Adaptation to Substrate Stiffness. *Proc. Natl. Acad. Sci. U. S. A.* **2012**, *109*, 6933−6938.

(9) Liu, K.; Jiang, L. Bio-Inspired Design of Multiscale Structures for Function Integration. *Nano Today* **2011**, *6*, 155−175.

(10) Asayesh, F.; Zarabadi, M. P.; Greener, J. A New Look at Bubbles During Biofilm Inoculation Reveals Pronounced Effects on Growth and Patterning. *Biomicrofluidics* **2017**, *11*, 064109.

(11) Dean, B.; Bhushan, B. Shark-Skin surfaces for Fluid-Drag Reduction in Turbulent Flow: a Review. *Philos. Trans. R. Soc., A* **2010**, *368*, 4775−4806.

(12) Guo, Z.; Liu, W. Biomimic from the Superhydrophobic Plant Leave in Nature: Binary Structure and Unitary Structure. *Plant Sci.* **2007**, *172*, 1103−1112.

(13) Feng, L.; Zhang, Y.; Cao, Y.; Ye, X.; Jiang, L. The Effect of Surface Microstructures and Surface Compositions on the Wettabilities of Flower Petals. *Soft Matter* **2011**, *7*, 2977−2980.

(14) Fratzl, P.; Barth, F. G. Biomaterial Systems for Mechanosensing and Actuation. *Nature* **2009**, *462*, 442−448.

(15) Bico, J.; Roman, B.; Moulin, L.; Boudaoud, A. Adhesion: Elastocapillary Coalescence in Wet Hair. *Nature* **2004**, *432*, 690−690.

(16) Yeh, Y.-H.; Cho, K.-H.; Chen, L.-J. Effect of Softness of Polydimethylsiloxane on the Hydrophobicity of Pillar-Like Patterned Surfaces. *Soft Matter* **2012**, *8*, 1079−1086.

(17) Nill, P.; Goehring, N.; Loeffler, R.; Peschel, A.; Kern, D. P. Studying Bacterial Adhesion Forces: Staphylococcus Aureus on Elastic Poly (Dimethyl) Siloxane Substrates. *Microelectron. Eng.* **2011**, *88*, 1825−1827.

(18) Pokroy, B.; Kang, S. H.; Mahadevan, L.; Aizenberg, J. Self-Organization of a Mesoscale Bristle Into Ordered, Hierarchical Helical Assemblies. *Science* **2009**, *323*, 237−240.

(19) Chandra, D.; Yang, S. Stability of High-Aspect-Ratio Micropillar Arrays Against Adhesive and Capillary Forces. *Acc. Chem. Res.* **2010**, *43*, 1080−1091.

(20) Chandra, D.; Yang, S. Capillary-Force-Induced Clustering of Micropillar Arrays: is it Caused by Isolated Capillary Bridges or by the Lateral Capillary Meniscus Interaction Force? *Langmuir* **2009**, *25*, 10430−10434.

(21) Roman, B.; Bico, J. Elasto-Capillarity: Deforming an Elastic Structure with a Liquid Droplet. *J. Phys.: Condens. Matter* **2010**, *22*, 493101.

(22) Marchand, A.; Weijs, J. H.; Snoeijer, J. H.; Andreotti, B. Why is Surface Tension a Force Parallel to the Interface? *Am. J. Phys.* **2011**, *79*, 999−1008.

(23) Weijs, J. H.; Andreotti, B.; Snoeijer, J. H. Elasto-Capillarity at the Nanoscale: on the Coupling between Elasticity and Surface Energy in Soft Solids. *Soft Matter* **2013**, *9*, 8494−8503.

(24) Yang, M. T.; Fu, J.; Wang, Y.-K.; Desai, R. A.; Chen, C. S. Assaying Stem Cell Mechanobiology on Microfabricated Elastomeric Substrates with Geometrically Modulated Rigidity. *Nat. Protoc.* **2011**, *6*, 187−213.

(25) Wei, Z.; Schneider, T.; Kim, J.; Kim, H.-Y.; Aizenberg, J.; Mahadevan, L. Elastocapillary Coalescence of Plates and Pillars. *Proc. R. Soc. London, Ser. A* **2015**, *471*, 20140593.

(26) Ledesma-Aguilar, R.; Laghezza, G.; Yeomans, J. M.; Vella, D. Using Evaporation to Control Capillary Instabilities in Micro-Systems. *Soft Matter* **2017**, *13*, 8947−8956.

(27) Jahed, Z.; Shahsavan, H.; Verma, M. S.; Rogowski, J. L.; Seo, B. B.; Zhao, B.; Tsui, T. Y.; Gu, F. X.; Mofrad, M. R. K. Bacterial Networks on Hydrophobic Micropillars. *ACS Nano* **2017**, *11*, 675−683.

(28) Chew, S. C.; Kundukad, B.; Teh, W. K.; Doyle, P.; Yang, L.; Rice, S. A.; Kjelleberg, S. Mechanical Signatures of Microbial Biofilms in Micropillar-Embedded Growth Chambers. *Soft Matter* **2016**, *12*, 5224−5232.

(29) Biais, N.; Ladoux, B.; Higashi, D.; So, M.; Sheetz, M. Cooperative Retraction of Bundled Type IV Pili Enables Nanonewton Force Generation. *PLoS Biol.* **2008**, *6*, 1−7.

(30) Ng, D.; Harn, T.; Altindal, T.; Kolappan, S.; Marles, J. M.; Lala, R.; Spielman, I.; Gao, Y.; Hauke, C. A.; Kovacikova, G.; Verjee, Z.; Taylor, R. K.; Biais, N.; Craig, L. The Vibrio cholerae Minor Pilin

DOI: 10.1021/acsabm.8b00176
ACS Appl. Bio Mater. XXXX, XXX, XXX−XXX

503 TcpB Initiates Assembly and Retraction of the Toxin-Coregulated
504 Pilus. *PLoS Pathog.* **2016**, *12*, 1−31.
505 (31) Susarrey-Arce, A.; Marin, A.; Massey, A.; Oknianska, A.; Díaz-
506 Fernandez, Y.; Hernández-Sánchez, J. F.; Griffiths, E.; Gardeniers, J.
507 G. E.; Snoeijer, J. H.; Lohse, D.; Raval, R. Pattern Formation by
508 Staphylococcus Epidermidis via Droplet Evaporation on Microoillars
509 Arrays at a Surface. *Langmuir* **2016**, *32*, 7159−7169.
510 (32) Hochbaum, A. I.; Aizenberg, J. Bacteria Pattern Spontaneously
511 on Periodic Nanostructure Arrays. *Nano Lett.* **2010**, *10*, 3717−3721.
512 (33) Li, X.; Cheung, G. S.; Watson, G. S.; Watson, J. A.; Lin, S.;
513 Schwarzkopf, L.; Green, D. W. The Nanotipped Hairs of Gecko Skin
514 and Biotemplated Replicas Impair and/or Kill Pathogenic Bacteria
515 with High Efficiency. *Nanoscale* **2016**, *8*, 18860−18869.
516 (34) Kim, P.; Epstein, A. K.; Khan, M.; Zarzar, L. D.; Lipomi, D. J.;
517 Whitesides, G. M.; Aizenberg, J. Structural Transformation by
518 Electrodeposition on Patterned Substrates (STEPS): A New Versatile
519 Nanofabrication Method. *Nano Lett.* **2012**, *12*, 527−533.
520 (35) Pokroy, B.; Epstein, A. K.; Persson-Gulda, M. C. M.; Aizenberg,
521 J. Fabrication of Bioinspired Actuated Nanostructures with Arbitrary
522 Geometry and Stiffness. *Adv. Mater.* **2009**, *21*, 463−469.
523 (36) Hadjittofis, A.; Lister, J. R.; Singh, K.; Vella, D. Evaporation
524 Effects in Elastocapillary Aggregation. *J. Fluid Mech.* **2016**, *792*, 168−
525 185.
526 (37) Haiko, J.; Westerlund-Wikström, B. The Role of the Bacterial
527 Flagellum in Adhesion and Virulence. *Biology* **2013**, *2*, 1242−1267.
528 (38) Hizal, F.; Choi, C.-H.; Busscher, H. J.; van der Mei, H. C.
529 Staphylococcal Adhesion, Detachment and Transmission on Nano-
530 pillared Si Surfaces. *ACS Appl. Mater. Interfaces* **2016**, *8*, 30430−
531 30439.
532 (39) Susarrey-Arce, A.; Sorzabal-Bellido, I.; Oknianska, A.; McBride,
533 F.; Beckett, A. J.; Gardeniers, J. G. E.; Raval, R.; Tiggelaar, R. M.; Diaz
534 Fernandez, Y. A. Bacterial Viability on Chemically Modified Silicon
535 Nanowire Arrays. *J. Mater. Chem. B* **2016**, *4*, 3104−3112.

DOI: 10.1021/acsabm.8b00176
ACS Appl. Bio Mater. XXXX, XXX, XXX−XXX